AIAA JOURNAL
Vol. 30, No. 5, May 1992

Free Vibrations of Delaminated Beams

M.-H. H. Shen*
Ohio State University, Columbus, Ohio 43210
and
J. E. Grady†
NASA Lewis Research Center, Cleveland, Ohio 44135

Free vibration of laminated composite beams is studied. The effect of interply delaminations on natural frequencies and mode shapes is evaluated both analytically and experimentally. A generalized variational principle is used to formulate the equation of motion and associated boundary conditions for the free vibration of a composite beam with a delamination of arbitrary size and location. The effect of coupling between longitudinal vibration and bending vibration is considered. This coupling effect is shown to significantly effect the calculated natural frequencies and mode shapes of the delaminated beam.

Nomenclature

A = beam cross-sectional area
b = half-breadth of rectangular beam
d = half-depth of rectangular beam
d_1 = delamination location along the thickness of the beam
E^* = composite bending modulus
f = nodal displacement vector, $(w,\beta,u)^T$
G^* = composite shear modulus
h = laminate thickness
I = cross-sectional area moment of inertia
J = functional integral
$[K_e]$ = global stiffness matrix
$[k_i]$ = element stiffness matrix
l_s = length of subbeam, $\equiv l/M$
l_1 = left crack tip location
l_2 = right crack tip location
M = number of subbeams
$[M_e]$ = global mass matrix
$[m_i]$ = element mass matrix
t = ply thickness
u = nodal longitudinal displacement vector
u_i = displacement components, u,v,w
$\hat{u}(x)$ = longitudinal deflection amplitude
V = volume
w = nodal transverse displacement vector
$w(x,t)$ = bending deflection
$\hat{w}(x)$ = bending deflection amplitude
β = shear angle
$\hat{\beta}$ = shear angle amplitude
β = nodal shear angle vector
δ_{ij} = Kronecker's delta, 1 for $i=j$; 0 for $i \neq j$
ϵ_{ij} = strain tensor component
η = position coordinate along a subbeam
ξ = x/l
ρ = mass density
σ_{ij} = stress tensor component
ω_c = natural frequency of delaminated beam
ω_{uc} = natural frequency of undelaminated beam

Superscripts

$\dot{}$ = $\partial/\partial t$
$'$ = $\partial/\partial x$

Received Feb. 14, 1991; presented as Paper 91-1241 at the AIAA/ASME/ASCE/AHS Structures, Structural Dynamics, and Materials Conference, Baltimore, MD, April 8-10, 1991; revision received July 31, 1991; accepted for publication Aug. 1, 1991.

*Assistant Professor, Department of Aeronautical and Astronautical Engineering.
†Aerospace Engineer. Member AIAA.

Introduction

THE use of composite materials has been increasing consistently in aerospace applications due to their high specific stiffness and strength. However, the mechanical properties of composite materials may degrade severely in the presence of damage. This damage may occur as a consequence of imperfections introduced during the manufacturing process or it may result from external loads occurring during the operational life, such as impact by foreign objects.

A considerable amount of research effort has been expended in attempting to understand and model the failure processes of composite materials. Such a task is complicated by the fact that damage in composite materials may grow as a combination of several failure modes such as matrix cracking, fiber pullout, fiber fracture, or delamination.[1] Delamination is one of the most common failure modes of composite materials and can potentially be the most damaging. Numerous researchers[2-12] have studied various aspects of the delamination process analytically and experimentally. Most of these studies were focused on either the initiation or the propagation of delamination under in-plane static or fatigue loadings. In comparison, little research has been done to determine the changes in dynamic response of composite materials caused by delamination.

Recently, several studies have been conducted in the area of vibration behavior. The effect of delamination on vibration properties of composite beams was studied by Grady and Meyn[13] and Lee et al.[14] Their experimental measurements showed that the natural frequencies and damping of composite test specimens were significantly affected by the introduction of an interfacial delamination. Because of the difficulty of mathematical modeling, the results of these tests were compared to calculations from finite element approach only.[13] The possibility of determining the integrity of composite beams from measured dynamic behavior was also proposed.[14] Free vibration of a laminated composite beam with a one-dimensional delamination was also studied by Ramkumar et al.[15] Their analytical model predicted a severe drop in the natural frequencies due to delamination, which was found to be inconsistent with experimental results. They attributed this discrepancy to the effect of contact between the delamination surfaces. However, this explanation has never been validated. Recently, Wang et al.[16] and Yin and Jane[17] have improved this analytical model by including the effect of coupling between the longitudinal and flexural motion in the delaminated plies. With the inclusion of coupling, the results were in good agreement with experimental measurements.

The objective of the proposed work is to further develop an effective mathematical model for determining the natural frequencies and corresponding mode shapes for composite beams with a delamination. This model is based on cracked beam theories[18-20] derived using Timoshenko beam theory and gen-

eral kinematic assumptions that account for the coupling effects just mentioned. A corresponding experimental study is also carried out to verify the analytical predictions. The use of this new theoretical model to identify the delamination position and size from changes in the natural frequencies and mode shapes of the beam is also discussed.

Theoretical Development

The geometry of the delaminated beam is shown in Fig. 1. The delamination is assumed to be uniform through the width of the beam and located arbitrarily, as defined by the parameters l_1, l_2, and d_1. The objective of the present theoretical model is to relate these parameters to the natural frequencies and mode shapes of the delaminated composite. For clarity, the theoretical formulations for the delaminated and undelaminated regions are derived separately, as follows.

Undelaminated Region

In the undelaminated regions, indicated by beams 1 and 3 in Fig. 1, only transverse vibration is considered. The assumptions using the Timoshenko beam theory to include shear deformation effects are summaried as the following:

$$
\begin{aligned}
&u_y = 0, \quad u_z = w(x,t), \quad u_x = -z(w' + \beta)\\
&p_x = 0, \quad p_y = 0, \quad p_z = P(x,t)\\
&\epsilon_{xx} = u', \quad \epsilon_{xz} = -\beta\\
&\epsilon_{yy} = \epsilon_{zz} = -\nu\epsilon_{xx}\\
&\epsilon_{xy} = \epsilon_{yz} = 0\\
&\sigma_{xx} = \sigma_{xx}(x,z,t), \quad \sigma_{xz} = \sigma_{xz}(x,z,t)\\
&\sigma_{yy} = \sigma_{zz} = \sigma_{xy} = \sigma_{yz} = 0\\
&X_x = X_y = X_z = 0
\end{aligned}
\tag{1}
$$

where u_i are the displacements referring to cartesian axes x, y, z; σ and ϵ represent stress and strain; β is the angle due to shear force; and X_i and p_i are the body forces and velocity components, respectively.

In this work, the Hu-Washizu principle is modified to include the virtual work done by the inertial forces. This yields the following functional:

$$
\begin{aligned}
J = \int_{t_1}^{t_2} \Bigg\{ \int_V \Bigg[&\rho p_i \dot{u}_i - \frac{1}{2}\rho p_i p_i - A(\epsilon_{ij})\\
&+ \left[\epsilon_{ij} - \frac{1}{2}(u_{i,j} + u_{j,i})\right]\sigma_{ij} + X_i u_i \Bigg] \, dV + \int_{S_1} \bar{g}_i u_i \, dS\\
&+ \int_{S_2} g_i(u_i - \bar{u}_i) \, dS \Bigg\} \, dt
\end{aligned}
\tag{2}
$$

where σ_{ij} and ϵ_{ij} are stress and strain components, X_i and p_i are the body forces and velocity components, respectively. (The indices $i,j = 1,2,3$ refer to the orthogonal directions x,y,z, respectively.) ρ is the mass density, $A(\epsilon_{ij})$ the strain energy density function, g_i the respective surface tractions, V the total volume of the system, S its external surface, S_1 the traction prescribed boundary, and S_2 the displacement prescribed boundary. The overbarred quantities $\bar{g}_i$ and $\bar{u}_i$ denote the prescribed values of surface tractions and surface displacements, respectively.

The functional J of Eq. (2) has stationary values for the actual solution for the independent quantities u_i, p_i, ϵ_{ij}, and σ_{ij}. Therefore, from variational principle, for arbitrary independent variations of δu_i [within conditions $\delta u(t_1) = \delta u(t_2) = 0$], δp_i, $\delta\epsilon_i$, and $\delta\sigma_i$, the first variation of the functional J vanishes, i.e., $\delta J = 0$, and is listed as follows:

$$
\begin{aligned}
\delta J = \int_{t_1}^{t_2} \Bigg\{ \int_V \Bigg\{ &(\sigma_{ij,j} + X_i - \rho\dot{p}_i)\delta u_i + (\sigma_{ij} - A_{\epsilon,ij})\delta\epsilon_{ij}\\
&+ [\epsilon_{ij} - \tfrac{1}{2}(u_{i,j} + u_{j,i})]\delta\sigma_{ij} + [\rho\dot{u}_i - (\tfrac{1}{2}\rho p_i p_i)_{,pi}]\delta p_i \Bigg\} \, dV\\
&+ \int_{S_1} (\bar{g}_i - g_i)\delta u_i \, dS + \int_{S_2} (u_i - \bar{u}_i)\delta g_i \, dS \Bigg\} \, dt = 0
\end{aligned}
\tag{3}
$$

The kinematic assumptions (1) are substituted into formulation (3), whereby the problem is reduced to a form corresponding to the beam model. The equations of motion can be derived in terms of displacement w and shear angle β by

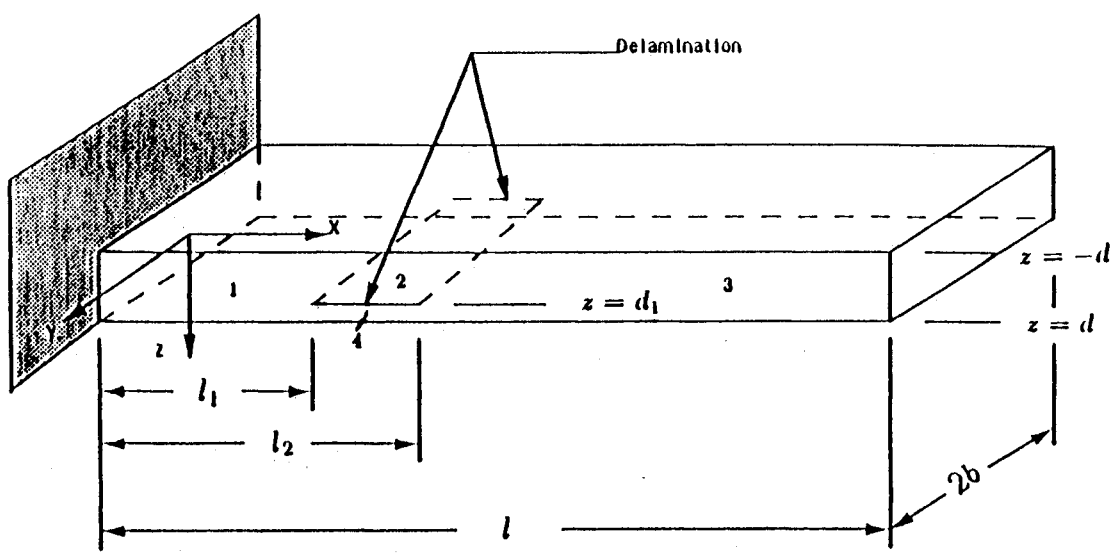

Fig. 1 Geometry of a composite laminated beam with a one-dimensional delamination.

subsequently integrating by parts each term of Eq. (7) and then integrating over the section. This gives

$$E^*I(w'''' + \beta''') + \rho A\ddot{w} = 0 \tag{4}$$

$$E^*I(w''' + \beta'') - A\kappa G^*\beta = 0 \tag{5}$$

along with the associated boundary conditions. Here, according to Ref. 21, $\kappa(= 0.7715)$ is the shear correction factor, and E^* and G^* are the effective beam bending and shear moduli, respectively.

Delaminated Region

In Fig. 1, the delaminated region is divided into the upper plies (beam 2) and the lower plies (beam 4). The governing equations of motion are the same as the equations, Eqs. (4) and (5), for the undelaminated region.

However, the effect of in-plane displacement u_2 and u_4 on the location of the neutral planes of beams 2 and 4, respectively, should be considered in order to achieve the matching conditions,

$$u_2 = e_2(w_2' + \beta_2), \qquad u_4 = e_4(w_4' + \beta_4) \tag{6}$$

at the left and right crack tips, respectively. The distance between neutral planes of the upper plies (beam 2) and undelaminated region is designated e_2. Similarly, e_4 is the distance between the neutral plane of the lower plies (beam 4) and undelaminated region. In the delaminated region, longitudinal motion is thereby coupled with bending motion, and the longitudinal vibration in the delaminated region changes the bending vibration of the delaminated beam. In other words, in order to describe the bending motion of the delaminated region (beams 2 and 4), in addition to analyze Eqs. (4) and (5), the governing equation for the longitudinal displacement u,

$$E^*Au'' - \rho A\ddot{u} = 0 \tag{7}$$

must also be included.

Two mathematical models are used in the present study. In the first model (model A), the crack interfaces are assumed to be in contact along the delaminated region throughout the vibration, and the coupling effect is accounted for in both the upper and lower plies of the delaminated region. Therefore, coupling between in-plane and transverse displacements described occurs throughout the entire delaminated region. In the second model (model B), contact between the delamination surfaces is neglected. Therefore, in-plane motion is not affected by bending, and coupling only occurs at the boundaries of the delamination (i.e., the crack tips). In addition, the effects associated with impact, friction, and penetration between the two crack faces are neglected for simplicity.

Application to Cantilevered Composite Beams

To test the accuracy of the present analytical model, the modes of free vibration of laminated composite beams with uniform one-dimensional delaminations have been examined. Following the diagram in Fig. 1, the example considered here is that of a rectangular, cantilevered beam with uniform cross section, of depth $2d$ and breadth $2b$. The delamination, of length $l_2 - l_1$, is located a distance d_1 from the neutral axis. Assuming simple harmonic motion, we take $w(x,t) = \hat{w}(x)e^{j\omega_c t}$, $\beta(x,t) = \hat{\beta}(x)e^{j\omega_c t}$, and $u(x,t) = \hat{u}(x)e^{j\omega_c t}$, which give

$$E_i^*I_i(\hat{w}_i'''' + \hat{\beta}_i'''') - \omega_c^2\rho A_i\hat{w}_i = 0, \qquad i = 1, \ldots, 4 \tag{8}$$

$$E_i^*I_i(\hat{w}_i''' + \hat{\beta}_i'') - A\kappa G_i^*\hat{\beta}_i = 0, \qquad i = 1, \ldots, 4 \tag{9}$$

$$E_i^*A_i\hat{u}_i'' - \omega_c^2\rho A_i\hat{u}_i = 0, \qquad i = 2, 4 \tag{10}$$

Results are thereby obtained for the natural frequencies and mode shapes in terms of delamination size and location.

Test Specimen Fabrication

Seventeen laminated plates of dimensions 6×12 in. were fabricated from T300/934 graphite/epoxy prepreg, supplied by ICI/Fiberite. Each laminate was laid up in an eight-ply $[0/90]_{2s}$ construction and cured using the supplier's recommended cure cycle. Individual test specimens, of nominal dimension $10 \times 0.5 \times 0.0435$ in., were cut from the laminates with a water knife that has a tolerance of ± 0.005 in. on all dimensions. Interply delaminations were simulated by inserting a 0.001-in.-thick teflon strip between selected plies of each laminate prior to curing. For comparison, one laminate was fabricated with no delamination.

Using a pair of calipers accurate to ± 0.0005 in., thickness measurements were taken of 120 individual test specimens cut from the 17 different laminates that were fabricated for this study. Of the specimens, 75% had thicknesses in the range $0.042 < h < 0.045$ or a variation of approximately $\pm 3.5\%$ from the average thickness of 0.0432 in. From Eq. (8), ω varies with $h^{3/2}$, so the variation in specimen thickness results in a $\pm 4.5\%$ uncertainty in the natural frequencies.

Vibration Testing

The apparatus shown in Fig. 2 was used to measure the resonant frequencies for the fundamental vibration mode of each of the test specimens. Each specimen was clamped along half of its span, as shown in the figure, to simulate a 5-in.-long, 0.5-in.-wide cantilevered beam with a single, uniform, through-width delamination centered at midspan. Within each laminate, a delamination of length 1, 2, 3, or 4 in. was embed-

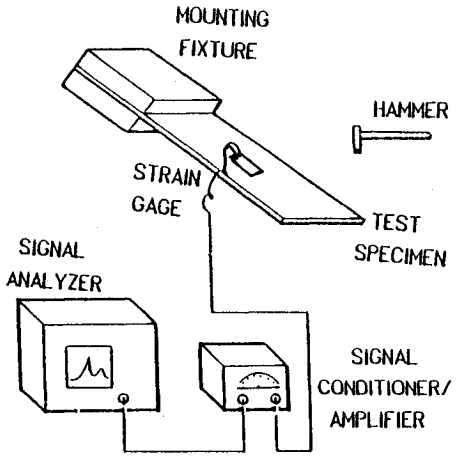

Fig. 2 Experimental apparatus for frequency measurement.

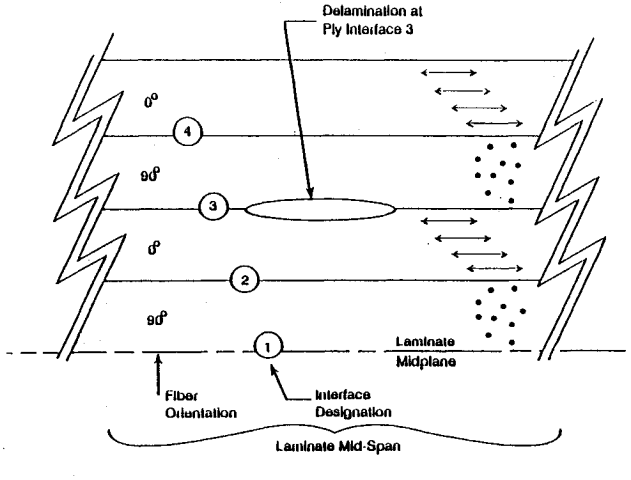

Fig. 3 Location of embedded flaw in composite laminate.

ded along one of the four ply interfaces shown in Fig. 3. Therefore, 16 different specimen types were tested, each with a different delamination size/location combination. Three replicates of each specimen configuration were tested to determine the measurement variability.

An electrical resistance strain gauge (type ED-DY-062AP-350) was mounted on each test specimen, 0.5 in. from the cantilevered support, and oriented longitudinally to measure flexural strain. A single-channel digital signal analyzer was used to record the transient strain response due to an impulsive force applied at the free end of the specimen. The first 8 s of the free vibration response was digitally sampled at a rate of 5120 samples/s. The frequency response, calculated from a fast Fourier transform of the time domain data, therefore had a resolution of 0.125 Hz, which corresponds to an inherent measurement error of approximately 0.375% for the lowest mode. The fundamental resonant frequency was identified by locating the first peak in the frequency response curve.

The first mode shape of each specimen type was measured photographically. Uninstrumented test specimens were centrally clamped to the actuator of a 100-lb capacity shaker, which divided the 10-in.-long specimens into two identical cantilevered beams of dimensions $5 \times 0.5 \times 0.0435$ in. The frequency of the sinusoidal forcing function was manually increased until the test specimen vibrated in its fundamental mode, as shown in Fig. 4. Because of the symmetrical displacement shape of the test specimen, an effectively clamped boundary condition is maintained at the central support point.

The mode shape was photographed with a black-and-white polaroid camera by choosing a shutter speed such that the film was exposed for approximately one cycle of motion; that is, the shutter was open for a time Δt given by

$$\Delta t = 1/\omega \tag{11}$$

where ω is the resonant frequency. While the shutter was open, the test specimen was illuminated by a strobe light that cycled on and off at a frequency Ω, chosen such that

$$\Omega = N\omega \tag{12}$$

where N is the approximate number of multiple exposures of the mode shape that are required. In this case, $N = 6$ was used, which gave typical results like that shown in the photograph in Figs. 5 for a test specimen with no delamination. Because of symmetry, only one-half of the vibrating test specimen is photographed.

Local Rayleigh-Ritz Method

Numerical integration of the mode shapes for the undelaminated beam are normally used to generate the mass and stiffness coefficients used in the Galerkin procedure. In this case, however, numerical integration is computationally intractable because these mode shapes include hyperbolic functions. This makes the Galerkin procedure impractical, particularly when many modes are required.

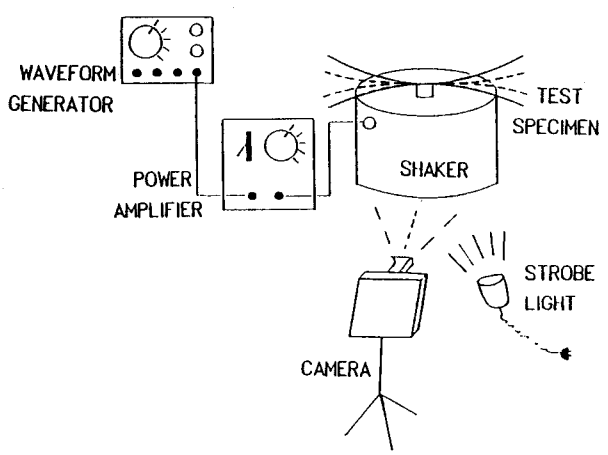

Fig. 4 Experimental apparatus for more shape measurement.

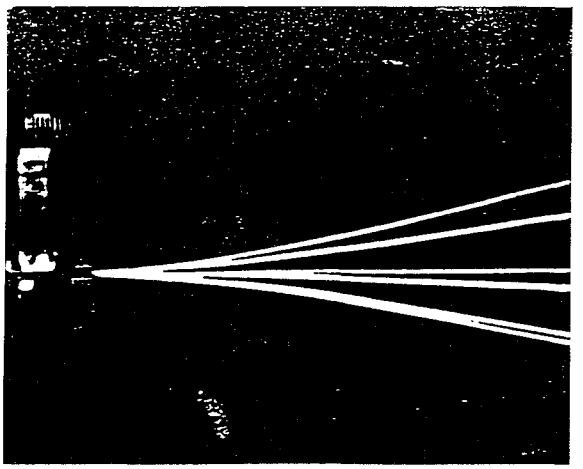

a) Photograph

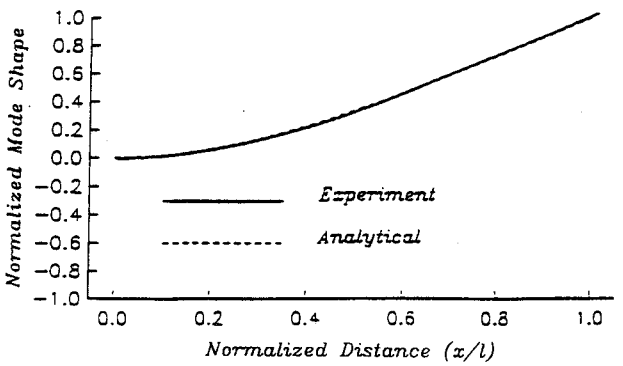

b) Comparison

Fig. 5 First bending mode shape of an undelaminated cantilevered beam.

To circumvent this problem, a local Rayleigh-Ritz method is used to calculate a piecewise continuous fit to the deflection shape. The displacements, $\hat{w}$, $\hat{\beta}$, and $\hat{u}$ are approximated by using cubic and linear polynomials defined over specific segments of the structure, here it is called subbeam. The coefficients of the polynomials are determined uniquely in terms of the displacements at the endpoints. The displacements at a point within the ith subbeam are approximated as

$$\hat{w}_i(\eta) = \boldsymbol{F}^T(\eta)\boldsymbol{w}_i, \qquad 0 \le \eta \le l_s \tag{13}$$

$$\hat{\beta}_i(\eta) = \boldsymbol{H}^T(\eta)\boldsymbol{\beta}_i, \qquad 0 \le \eta \le l_s \tag{14}$$

$$\hat{u}_i(\eta) = \boldsymbol{H}^T(\eta)\boldsymbol{u}_i, \qquad 0 \le \eta \le l_s \tag{15}$$

where $\boldsymbol{F} = [F_1, F_2, F_3, F_4]^T$ and $\boldsymbol{H} = [H_1, H_2]^T$ are vectors of prescribed (shape) functions of position and $\boldsymbol{w}_i$, $\boldsymbol{\beta}_i$, and $\boldsymbol{u}_i$ are vectors of end transverse deflection and its slope, shear angle, and longitudinal displacement for the ith subbeam. The shape functions $(F_j)_{j=1,\ldots,4}$ and $(H_j)_{j=1,2}$ are listed in the Appendix. This piecewise polynomial interpolation amounts to a finite element solution of the differential equations (8-10) for the delaminated beam. In this analysis, a local Rayleigh-Ritz model with six shape functions, M identical subbeams, M_d subbeams in the delamination region, and a total of $3(M-1) + 2(M_d - 1)$ degrees of freedom is used.

The free vibration eigenvalue problem is expressed as

$$[K_e]f - \omega_c^2[M_e]f = 0 \tag{16}$$

Table 1 Properties of the composite beams (each ply)

E_{11}	$= 19.5 \times 10^6$ psi
E_{22}	$= 1.5 \times 10^6$ psi
G_{12}	$= 0.725 \times 10^6$ psi
ν_{12}	$= 0.33$
ρ	$= 1.3821 \times 10^{-4}$ lb-s^2/in.^{4}

where $f = (w, \beta, u)^T$ is the vector of nodal displacements, and $[K_e]$ and $[M_e]$ are the global stiffness and mass matrices for the entire beam, respectively. The assembly process used to obtain these matrices is symbolically described by

$$(f, [K_e], [M_e]) = \sum_{i=1}^{M} (f_i, [k_i], [m_i]) \tag{17}$$

where f_i, $[k_i]$, and $[m_i]$ are the nodal displacement, stiffness and mass matrices, respectively, for the ith subbeam, and the summation extends over all $M + M_d$ subbeams. The mass and stiffness matrices of the ith subbeam, in the local coordinate system, are

$$[m_i] = \rho A_i \begin{bmatrix} m_6 & 0 & 0 \\ 0 & m_1 & 0 \\ 0 & 0 & 0 \end{bmatrix} \tag{18}$$

$$[k_i] = (E_i^* I_i) \begin{bmatrix} k_6 & 0 & 0 \\ 0 & k_1 & k_2 \\ 0 & k_3 & k_4 \end{bmatrix} \tag{19}$$

where the individual elements of the stiffness and mass matrices are given in the Appendix.

The stiffness and mass matrices have dimension 6×6 for the subbeams located in the undelaminated region and 8×8 in delaminated region.

The eigenvalue problem, Eq. (16), is then solved for an increasing number of subbeams M until a frequency convergence test was satisfied:

$$\max \left| \frac{\Delta \omega_i^M}{\omega_c^M} \right| < \epsilon \tag{20}$$

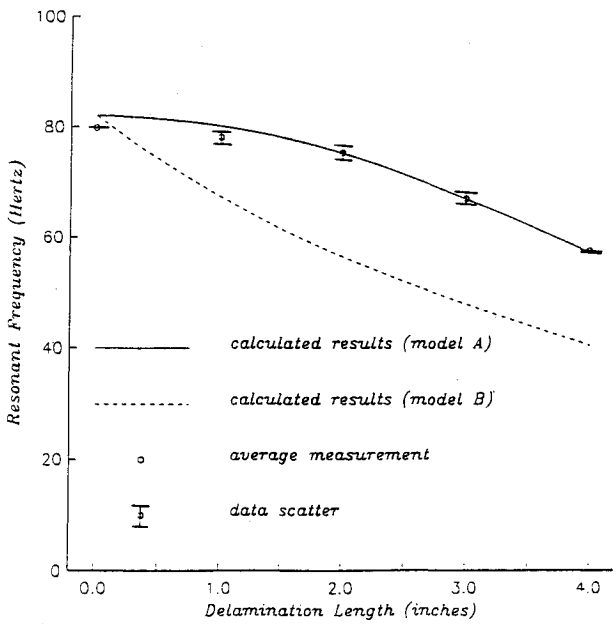

Fig. 6 First bending frequency for midplane delamination (interface 1).

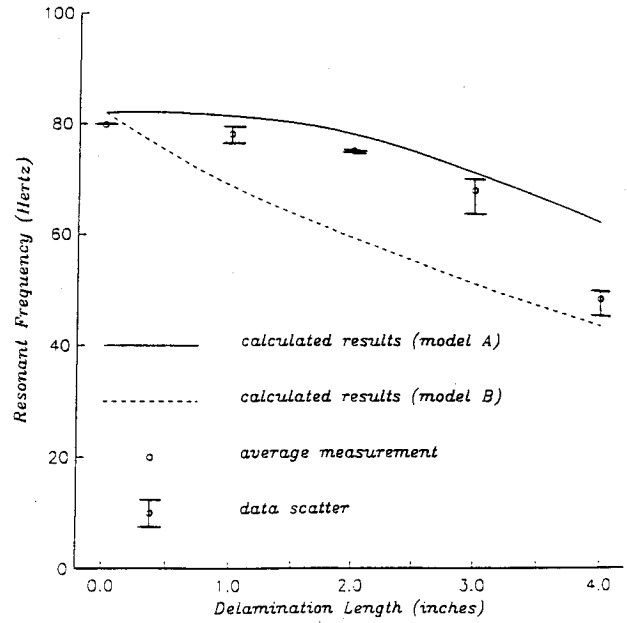

Fig. 7 First bending frequency for delamination along interface 2.

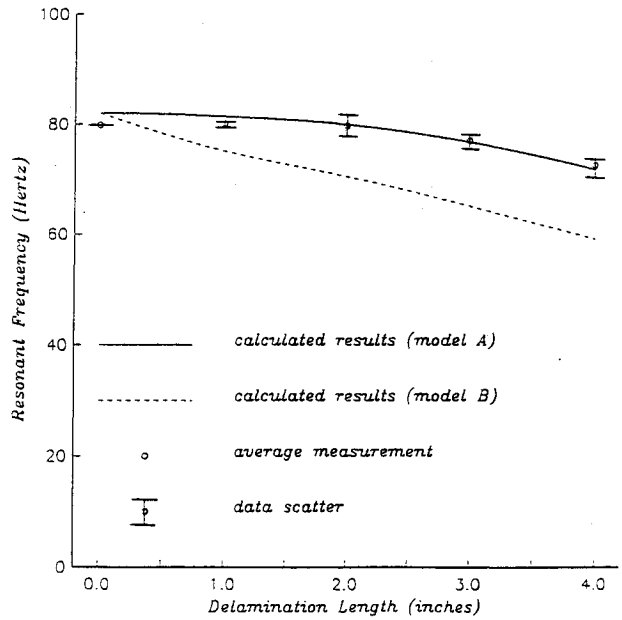

Fig. 8 First bending frequency for delamination along interface 3.

where $\Delta \omega_i^M$ is the change in the first frequency from the M-subbeam to the $(M+1)$-subbeam calculation, ω_c^M is the M-subbeam estimate of the first frequency of the delaminated beam, and ϵ is a small real number. For all cases presented in this paper, 100 subbeams were necessary to achieve convergence with $\epsilon = 2.0 \times 10^{-5}$.

Results and Discussion

The validity of this theoretical model is now demonstrated by applying it to a composite beam structure with embedded internal delaminations of varying size and at several different locations. Specifically, the material is a graphite fiber/epoxy matrix composite with ply properties as given in Table 1. The test specimens are cut from eight-ply laminates, laid up in a cross-ply, $[0/90]_{2s}$ configuration. It is important to note that the thickness of the beam used in the following theoretical analysis was 0.04 in., which was determined by adding the nominal thickness (0.005 in.) of the individual plies.

Natural Frequencies

Calculated results presented in Figs. 6–9 and Tables 2–5 show the effect of delamination size and interface location on the fundamental natural frequencies of the beam. Model A (solid line) is based on the assumption that longitudinal/flexural coupling exists along the entire length of the delamination, and model B (dashed line) assumes that coupling exists only at the two delamination crack tips. Data points indicate the average measured frequency from vibration tests of three different experimental specimens, which were tested as described earlier. The error bars indicate the measurement variation for the three tests. Data scatter increases slightly for the longer delaminations.

The results shown in Figs. 6–9 and Tables 2–5 indicate that model A gives relatively good agreement between the calcu-

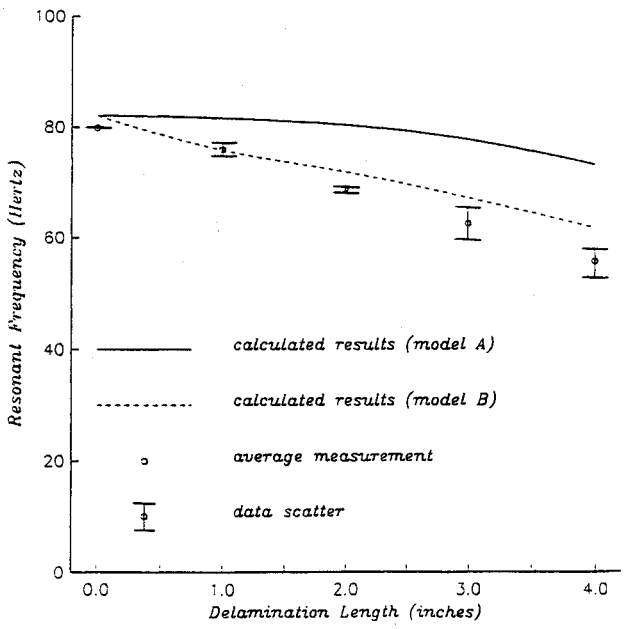

Fig. 9 First bending frequency for delamination along interface 4.

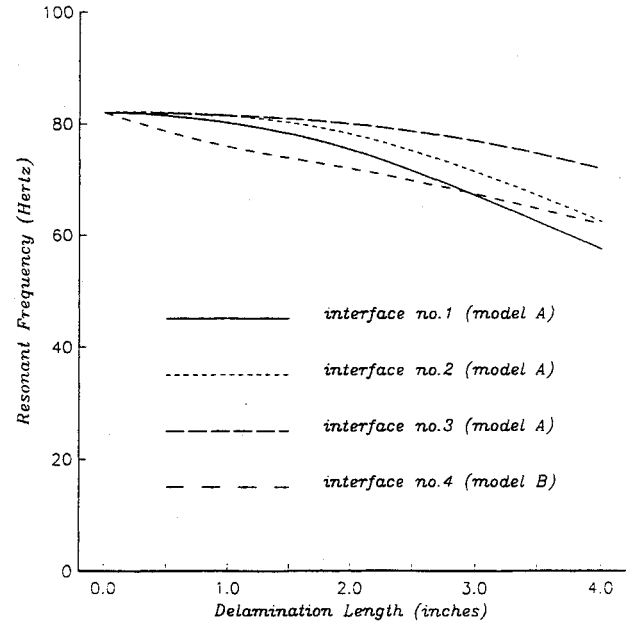

Fig. 10 First bending frequency in terms of interface.

Table 2 Fundamental resonant frequency for delamination along interface 1

$l_2 - l_1$,[a] in.	Specimen 1, Hz	Specimen 2, Hz	Specimen 3, Hz	Analytical model A	Analytical model B
0.0	79.875	79.875	79.750	82.042	82.042
1.0	78.376	79.126	77.001	80.133	67.363
2.0	74.375	75.000	76.751	75.285	56.479
3.0	68.250	66.250	66.375	66.936	47.898
4.0	57.623	57.502	57.501	57.239	40.586

[a]Delamination length.

Table 3 Fundamental resonant frequency for delamination along interface 2

$l_2 - l_1$,[a] in.	Specimen 1, Hz	Specimen 2, Hz	Specimen 3, Hz	Analytical model A	Analytical model B
0.0	79.875	79.875	79.750	82.042	82.042
1.0	78.375	78.375	76.626	81.385	68.776
2.0	75.126	75.250	75.001	78.103	59.438
3.0	64.001	70.001	69.876	71.159	51.180
4.0	45.752	49.751	49.502	62.121	43.860

[a]Delamination length.

Table 4 Fundamental resonant frequency for delamination along interface 3

$l_2 - l_1$,[a] in.	Specimen 1, Hz	Specimen 2, Hz	Specimen 3, Hz	Analytical model A	Analytical model B
0.0	79.875	79.875	79.750	82.042	82.042
1.0	79.625	80.125	80.625	81.461	75.137
2.0	79.500	81.875	77.875	79.932	70.416
3.0	75.625	77.125	78.125	76.712	65.058
4.0	73.376	73.627	70.376	71.663	59.131

[a]Delamination length.

Table 5 Fundamental resonant frequency for delamination along interface 4

$l_2 - l_1$,[a] in.	Specimen 1, Hz	Specimen 2, Hz	Specimen 3, Hz	Analytical model A	Analytical model B
0.0	79.875	79.875	79.750	82.042	82.042
1.0	75.375	75.250	77.250	81.598	75.834
2.0	69.376	68.001	69.375	80.383	71.881
3.0	65.375	59.625	—	77.698	67.181
4.0	52.750	57.876	56.251	73.147	61.704

[a]Delamination length.

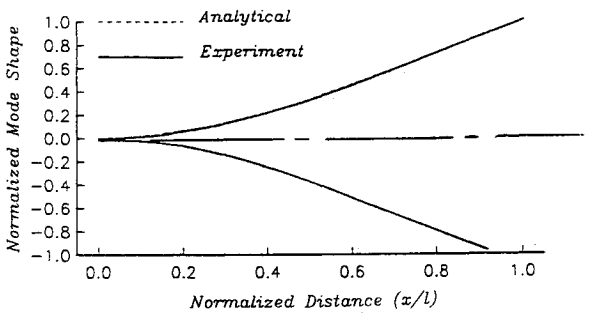

a) 1-in. delamination

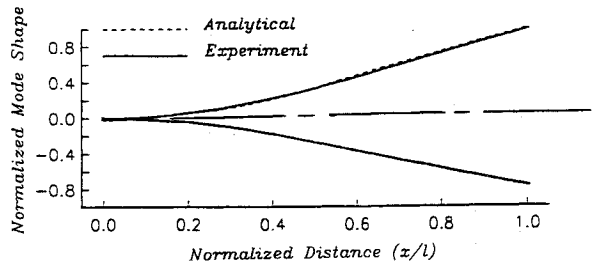

b) 2-in. delamination

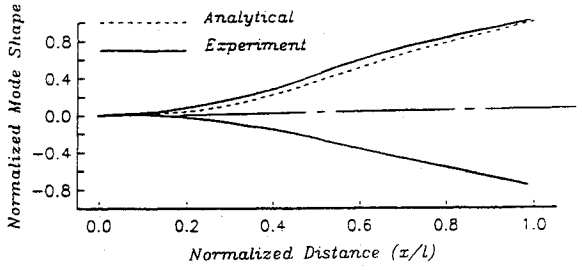

c) 3-in. delamination

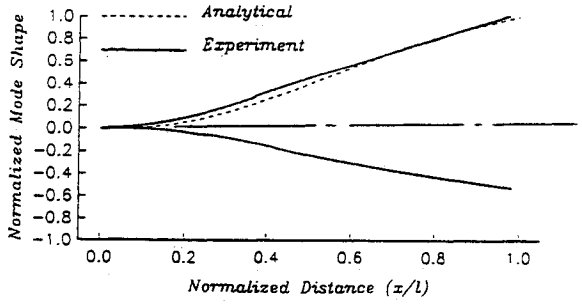

d) 4-in. delamination

Fig. 11 First bending mode shape of cantilevered beams with a delamination at interface 1.

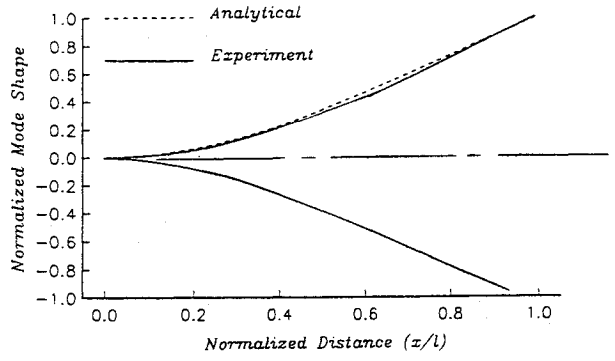

a) 1-in. delamination

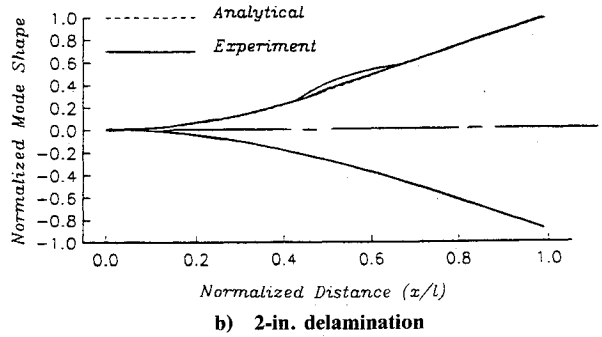

b) 2-in. delamination

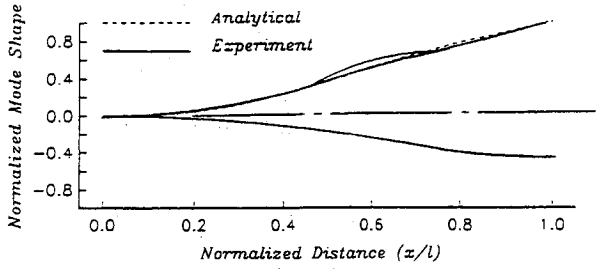

c) 3-in. delamination

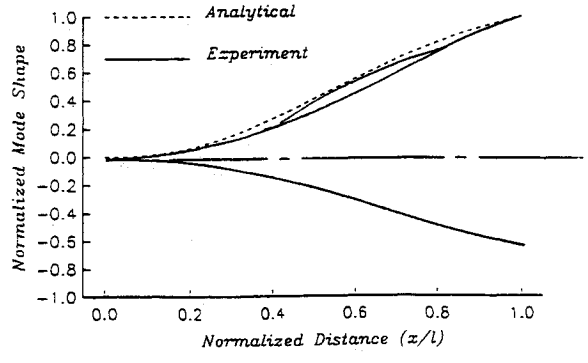

d) 4-in. delamination

Fig. 12 First bending mode shape of cantilevered beams with a delamination at interface 2.

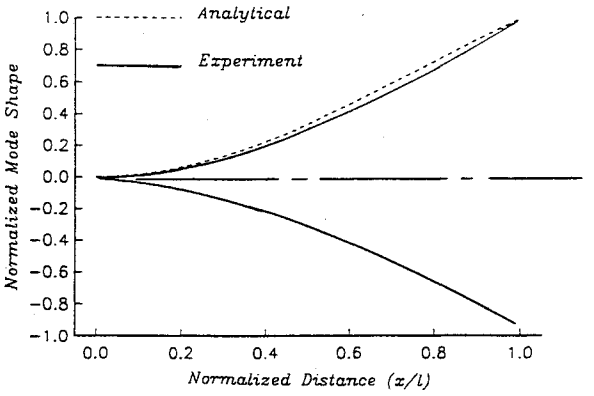

a) 1-in. delamination

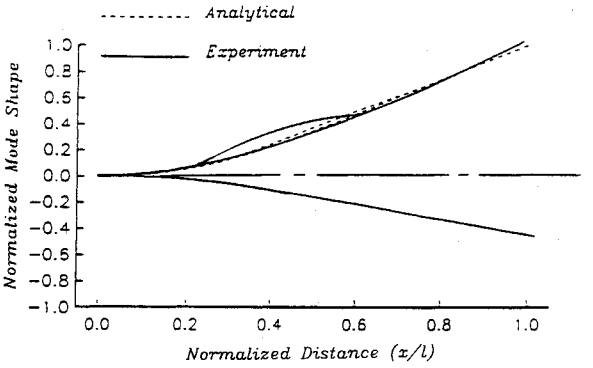

c) 3-in. delamination

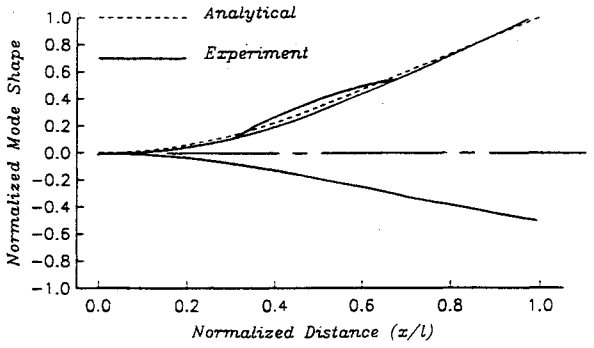

b) 2-in. delamination

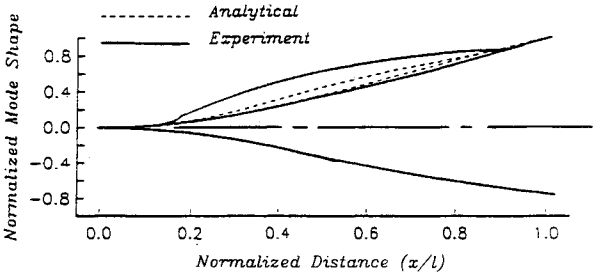

d) 4-in. delamination

Fig. 13 First bending mode shape of cantilevered beams with a delamination at interface 3.

lated frequencies and test results at three of the four interfaces. When the delamination lies along the outermost interface, model B gives the best agreement with test data. This indicates that the longitudinal/flexural coupling in the delaminated region is insignificant when the delamination lies between the outermost plies of the laminate. In all other cases, coupling significantly increases the vibration frequency. For short delaminations, the frequencies are relatively insensitive to delamination size; particularly for delaminations shorter than 1 in. (20% of the span). Both analysis and test results indicate that the sensitivity (i.e., slope) of the frequencies to delamination size increases with the length of the delamination for all interfacial locations. Figures 6 and 8 show excellent agreement between the calculated frequencies and the experimental results for delaminations along the midplane and interface 3, respectively. Figures 7 and 9 show that theoretical model slightly overestimates the measured frequencies when the delamination lies along interfaces 2 and 4.

The theoretical results from Figs. 6–9 are plotted together in Fig. 10. This figure shows clearly that the natural frequency is most sensitive to delaminations near the midplane of the laminate, and that the sensitivity generally decreases as the distance between the delamination and the midplane increases. This could be a result of the higher degree of coupling between the longitudinal and bending motion when the delamination lies closer to the midplane. For delaminations very close to the outer surface of the laminate (interface 4), however, the frequencies are most sensitive to delamination size, due to the lack of a longitudinal/flexural coupling effect, as discussed earlier.

Mode Shapes

The mode shapes of composite beams are also affected by the size and location of embedded delaminations. In this section, the calculated mode shapes are compared with those measured photographically for each of the 16 different combinations of delamination size/interface location examined in this study.

To compare the photographic results with theoretical calculations, the amplitude of the calculated mode shape was normalized such that the free-end displacement of the beam was the same as that measured experimentally. The maximum-amplitude deformed shape of each test specimen was then manually traced from multiple-exposure photographs of the fundamental mode shape similar to that shown in Figs. 5 for an undelaminated test specimen. The resulting comparisons are shown in Figs. 11–14. If the delamination is off the laminate midplane (interface 1), the deformation of the laminate depends on whether the delaminated plies are in longitudinal tension or compression. This is illustrated by the mode shape in Figs. 12 and 13, which is unsymmetric about the line $y = 0$ because the delamination opens under compression, but not under tension. The vibration amplitude is therefore higher during the compressive part of the cyclic motion because the delaminated plies do not contribute much bending stiffness to the laminate when they are in compression.

The calculated mode shapes are in close agreement with the experimental measurements for the compressive part of the vibration cycle. When the delamination is along a ply interface other than the laminate midplane (interfaces 2, 3, 4), a measurable crack opening forms in the delaminated region. This is evident in the experimental results shown in Figs. 12–14 and also appears in the calculated mode shapes for interface 4, although to a lesser extent. The calculations did not show a significant crack opening for the other interface locations. Experimental observations indicated that the relative magnitude of the crack opening displacement is dependent on the magnitude of the sinusoidal forcing function.

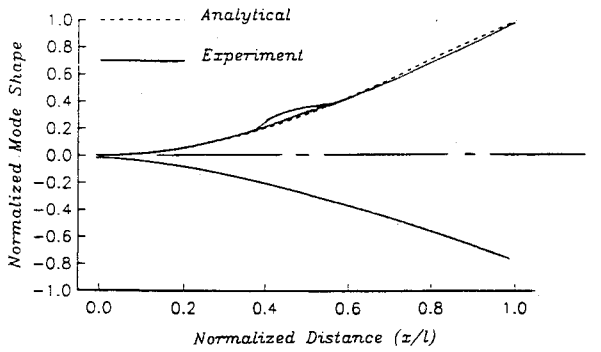

a) 1-in. delamination

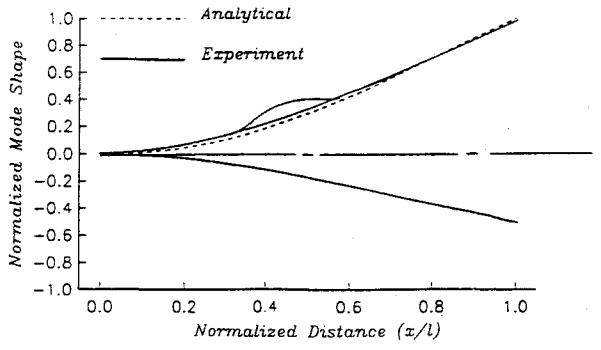

b) 2-in. delamination

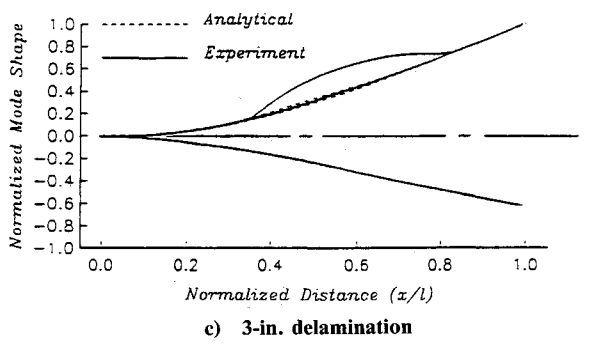

c) 3-in. delamination

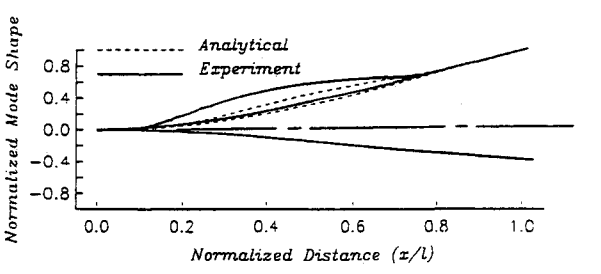

d) 4-in. delamination

Fig. 14 First bending mode shape of cantilevered beams with a delamination at interface 4.

Conclusions

A formulation for the flexural motion of a composite beam containing a one-dimensional delamination crack is presented. It is based on a key kinematic assumption made to satisfy the compatibility requirements in the vicinity of the delaminated region. The idea is to include the coupling between longitudinal vibration and bending vibration in the modes of vibration. This effect is found to significantly affect the modes of vibration.

The equation of motion and associated boundary conditions are derived under the generalized variational principle. The derivation procedure can be used for the cases of short beams, where the effect of shear stress concentration near the crack tips becomes important. The validity of the theory is established by examining dynamic response of a cantilevered composite beam. The analytical solutions show excellent agreement with experimental results. The effects of delaminations on frequency and mode shape are found to be very sensitive to delamination size and interface location.

The present theory could be extended easily to beams account for contact of delamination crack faces and therefore, the effects on delaminations to the higher mode is achievable. Other future work includes the development of an inverse analysis procedure to identify the delamination properties from dynamical measurements. Also, there is a need to extend the present method for modeling the delamination to two-dimensional plate and shell structures.

Appendix

The shape function for the subbeam equations (13-15) are given by

$$F_1 = 1 - 3\left(\frac{\eta}{l}\right)^2 + 2\left(\frac{\eta}{l}\right)^3, \qquad F_2 = \eta - 2\frac{\eta^2}{l} + \frac{\eta^3}{l^2}$$

$$F_3 = 3\left(\frac{\eta}{l}\right)^2 - 2\left(\frac{\eta}{l}\right)^3, \qquad F_4 = -\frac{\eta^2}{l} + \frac{\eta^3}{l^2}$$

$$H_1 = 1 - \frac{\eta}{l_s}, \qquad H_2 = \frac{\eta}{l_s}$$

The elements of the mass matrix, Eq. (18), for the individual subbeams are given by

$$[m_1] = \int_0^{l_s} \boldsymbol{F}^T\boldsymbol{F}\,\mathrm{d}\eta, \qquad [m_6] = \int_0^{l_s} \boldsymbol{H}^T\boldsymbol{H}\,\mathrm{d}\eta$$

and the elements of the stiffness matrix, Eq. (19), are given by

$$[k_1] = (E_i^* I_i)\int_0^{l_s} \boldsymbol{B}^T\boldsymbol{B}\,\mathrm{d}\eta, \quad [k_2] = (E_i^* I_i)\int_0^{l_s} \boldsymbol{B}^T\boldsymbol{P}\,\mathrm{d}\eta$$

$$[k_3] = E_i^* I_i\int_0^{l_s} \boldsymbol{P}^T\boldsymbol{B}\,\mathrm{d}\eta, \qquad [k_6] = E_i^* A_i\int_0^{l_s} \boldsymbol{P}^T\boldsymbol{P}\,\mathrm{d}\eta$$

$$[k_4] = E_i^* I_i\int_0^{l_s} \boldsymbol{P}^T\boldsymbol{P} + \,\mathrm{d}\eta + \kappa G_i^*\int_0^{l_s} \boldsymbol{H}^T\boldsymbol{H}\,\mathrm{d}\eta$$

where $\boldsymbol{P} = (d/d\eta)\boldsymbol{H}$ and $\boldsymbol{B} = (d^2/d^2\eta)\boldsymbol{F}$.

Acknowledgments

Part of this research work was conducted by M.-H. H. Shen at the Ohio Aerospace Institute. The experiments of this work were performed at NASA Lewis Research Center.

References

[1]Roderick, G. L., Everett, R. A., and Crews, J. H., "Debond Propagation in Composite-Reinforced Metals," *Fatigue of Composite Materials,* edited by J. R. Hancock, ASTM STP 569, American Society for Testing and Materials, Philadelphia, PA, 1975, pp. 295-306.

[2]Pagano, N. J., and Pipes, R. B., "Some Observations on the Interlaminar Strength of Composite Materials," *International Journal of Mechanical Sciences,* Vol. 15, No. 8, 1973, pp. 679-688.

[3]Sendeckyi, G. P., Stainaker, H. D., and Kleismit, R. A., *Fatigue of Filamentary Composite Materials,* edited by K. L. Reifsnider and K. N. Lauraitis, ASTM STP 636, American Society for Testing and Materials, Philadelphia, PA, 1977, pp. 123-140.

[4]Wang, S. S., "An Analysis of Delamination in Angle-Ply Fiber-Reinforced Composites," *Journal of Applied Mechanics,* Vol. 47, No. 1, 1980, pp. 64-70.

[5]Raju, I. S., and Crews, J. H., Jr., "Interlaminar Stress Singularities at a Straight Free Edge in Composite Laminates," *Computers and Structures,* Vol. 14, No. 1-2, 1981, pp. 21–28.

[6]Chia, H., Babcock, D., and Knauss, W. G., "One Dimensional Modelling of Failure in Laminated Plates by Delamination Bucking," *International Journal of Solids Structures,* Vol. 17, No. 11, 1981, pp. 1069–1083.

[7]Wang. S. S., and Choi, I., "The Interface Crack Between Dissimilar Anisotropic Composite Materials," *Journal of Applied Mechanics,* Vol. 50, No. 1, 1983, pp. 169–178.

[8]Whitney, J. M., "Characterization of Interlaminar Fracture Toughness," *Proceedings of the Eighth Annual Mechanics of Composites Review,* Air Wright Aeronautics Lab., AFWAL-TR-83-4005, Wright-Patterson AFB, OH, 1983, pp. 73–84.

[9]O'Brien, T. K., "Analysis of Local Delaminations and Their Influence on Composite Laminate Behavior," *Delamination and Debonding of Materials,* edited by W. S. Johnson, ASTM STP 876, American Society for Testing and Materials, Philadelphia, PA, 1985, pp. 282–297.

[10]Garg, A. C., "Intralaminar and Interlaminar Fracture in Graphite/Epoxy Laminates," *Engineering Fracture Mechanics,* Vol. 23, No. 4, 1986, pp. 719–733.

[11]Bottega, W. J., and Maewal, A., "Dynamics of Delamination Buckling," *International Journal of Nonlinear Mechanics,* Vol. 18, No. 6, 1983, pp. 449–463.

[12]Bottega, W. J., "Instability of a Partially Delaminated Surface Layer of an Oscillating Cylinder," *AIAA Journal,* Vol. 28, No. 11, 1990, pp. 2008–2011.

[13]Grady, J. E., and Meyn, E. H., "Vibration Testing of Impact-Damaged Composite Laminates," *Proceedings of the AIAA/ASME/ASCE/AHS/ASC 30th Structures, Structural Dynamics, and Materials Conference,* AIAA, Washington, DC, 1989, pp. 2186–2193; AIAA Paper 89-1411, 1989.

[14]Lee, B. T., Sun, C. T., and Liu, D., "An Assessment of Damping Measurement in the Evaluation of Integrity of Composite Beams," *Journal of Reinforced Plastics and Composites,* Vol. 6, April 1987, pp. 114–125.

[15]Ramkumar, R. L., Kulkarni, S. V., and Pipes, R. B., "Free Vibration Frequencies of A Delaminated Beam," *Proceedings of 34th Annual Technical Conference,* Reinforced/Composites Inst., Society of Plastics Industry Inc., Sec. 22-E, 1979, pp. 1–5.

[16]Wang, J. T. S., Liu, Y. Y., and Gibby, J. A., "Vibration of Split Beams," *Journal of Sound and Vibration,* Vol. 84, No. 4, 1982, pp. 491–502.

[17]Yin, W.-L., and Jane, K. C., "Vibration of A Delaminated Beam-Plate Relative to Buckled States," *Proceedings of the AIAA/ASME/ASCE/AHS 29th Structures, Structural Dynamics, and Materials Conference,* Vol. 2, AIAA, Washington, DC, 1988, pp. 860–870.

[18]Shen, M.-H. H., "Natural Modes of Cracked Beams and Identification of Cracks," Ph.D. Dissertation, Univ. of Michigan, Ann Arbor, MI, Aug. 1989.

[19]Shen, M.-H. H., and Pierre, C., "Natural Modes of Bernoulli-Euler Beams with Symmetric Cracks," *Journal of Sound and Vibration,* Vol. 138, No. 1, 1990, pp. 115–134.

[20]Shen, M.-H. H., and Pierre, C., "Free Vibrations of Beams with a Single-Edge Crack," *Journal of Sound and Vibration* (submitted for publication).

[21]Whitney, J. M., "Shear Correction Factors for Orthotropic Laminates Under Static Loading," *Journal of Applied Mechanics,* Vol. 40, No. 1, 1973, pp. 302–304.